Thermoelectric and mechanical properties of spark plasma sintered Cu3SbSe3 and Cu3SbSe4: Promising thermoelectric materials

Kriti Tyagi, Bhasker Gahtori, Sivaiah Bathula, Vijaykumar Toutam, Sakshi Sharma, Niraj Kumar Singh, and Ajay Dhar

Articles you may be interested in

Microstructure and mechanical properties of thermoelectric nanostructured n-type silicon-germanium alloys synthesized employing spark plasma sintering
Appl. Phys. Lett. **105**, 061902 (2014); 10.1063/1.4892879

Enhanced thermoelectric performance in spark plasma textured bulk n-type BiTe2.7Se0.3 and p-type Bi0.5Sb1.5Te3
Appl. Phys. Lett. **102**, 211901 (2013); 10.1063/1.4807771

High thermoelectric figure of merit in the Cu3SbSe4-Cu3SbS4 solid solution
Appl. Phys. Lett. **98**, 261911 (2011); 10.1063/1.3605246

Enhanced thermoelectric properties in CoSb 3 - x Te x alloys prepared by mechanical alloying and spark plasma sintering
J. Appl. Phys. **102**, 103717 (2007); 10.1063/1.2815671

High-performance Ag 0.8 Pb 18 + x SbTe 20 thermoelectric bulk materials fabricated by mechanical alloying and spark plasma sintering
Appl. Phys. Lett. **88**, 092104 (2006); 10.1063/1.2181197

Thermoelectric and mechanical properties of spark plasma sintered Cu₃SbSe₃ and Cu₃SbSe₄: Promising thermoelectric materials

Kriti Tyagi, Bhasker Gahtori, Sivaiah Bathula, Vijaykumar Toutam, Sakshi Sharma, Niraj Kumar Singh, and Ajay Dhar[a)]
CSIR-Network of Institutes for Solar Energy, Materials Physics and Engineering, CSIR-National Physical Laboratory, Dr. K. S. Krishnan Road, New Delhi 110012, India

We report the synthesis of thermoelectric compounds, Cu₃SbSe₃ and Cu₃SbSe₄, employing the conventional fusion method followed by spark plasma sintering. Their thermoelectric properties indicated that despite its higher thermal conductivity, Cu₃SbSe₄ exhibited a much larger value of thermoelectric figure-of-merit as compared to Cu₃SbSe₃, which is primarily due to its higher electrical conductivity. The thermoelectric compatibility factor of Cu₃SbSe₄ was found to be ∼1.2 as compared to $0.2 \, \mathrm{V}^{-1}$ for Cu₃SbSe₃ at 550 K. The results of the mechanical properties of these two compounds indicated that their microhardness and fracture toughness values were far superior to the other competing state-of-the-art thermoelectric materials. © *2014 AIP Publishing LLC*. [http://dx.doi.org/10.1063/1.4904996]

Electrical energy can be produced directly by harnessing waste-heat employing thermoelectric (TE) power generation; however, the limited efficiency of the existing TE materials limits their usage for commercial applications.[1] The efficiency of TE devices is strongly associated with the dimensionless figure-of-merit (ZT) of its constituent n- and p-type TE materials and can be increased by enhancing the ZT, which is defined as, $ZT = (\alpha^2 \sigma / \kappa) \, T$, where α is the Seebeck coefficient, σ is the electrical conductivity, and κ is the total thermal conductivity ($\kappa = \kappa_L + \kappa_e$, the lattice and electronic contributions, respectively). A high electrical conductivity, a large Seebeck coefficient, and low thermal conductivity are desired in order to realize a high-performance TE material.[2] It is well known that the best TE materials are narrow bandgap semiconductors,[3] and recently, several Cu–Sb–Se based ternary compounds have been found to exhibit promising thermoelectric properties.[4–7] Among these, Cu₃SbSe₃ and Cu₃SbSe₄ exhibit interesting electronic and thermal transport properties as both of these are narrow bandgap semiconductors.[6,8] Moreover, Cu₃SbSe₃ and Cu₃SbSe₄ have received considerable attention as potential TE materials, since experimental measurements have recently shown that Cu₃SbSe₃ exhibits an ultra-low and nearly temperature-independent lattice thermal conductivity.[5,7] Recently, many reports[5,9] have also appeared in literature on the thermoelectric properties of Cu₃SbSe₄ and Cu₃SbSe₃[10,11] compounds. On the other hand, apart from the ZT, the mechanical properties of these TE materials are also equally important especially for device fabrication wherein these TE materials have to withstand thermal stresses created due to rapid temperature cycling and gradients across its module TE elements. Hence, apart from their TE properties there is a need to determine their mechanical properties as well. Therefore, the objective of the current work is to study the TE

properties of Cu₃SbSe₃ and Cu₃SbSe₄ compounds and to provide an insight into their mechanical properties, both of which are equally important for their use for TE device applications in the mid-temperature range.

Experimental synthesis of Cu₃SbSe₃ has been reported elsewhere[5] and a similar methodology has been adopted for the synthesis of Cu₃SbSe₄. The density of both the samples, was measured using the conventional Archimedes principle and was found to be ∼98.6% of their theoretical density. The high densifications in both the samples are due to the rapid heating rates generated by Spark Plasma Sintering (SPS) used for synthesizing the materials. Further, nano-indentation on these samples was carried out employing Berkovich indentor using Multi-mode Atomic Force Microscope (AFM) (Bruker Ltd.,) with Nanoscope 5 controller. The deflection sensitivity was measured on sapphire surface after performing Force–Displacement (F-D) spectroscopy on the samples. In order to use a maximum set load, the AFM tip was engaged with an x-rotation of 12° with a small amplitude of 300 mV. To minimize the errors, all the measurements were carried out without disturbing the laser alignment on the cantilever. Indentation–fracture toughness analysis was carried out employing Vickers's micro hardness tester (Model: FM-e7, Make: Future Tech Corp., Japan).

Figs. 1(a) and 1(b) show the X-Ray Diffraction (XRD) patterns of Cu₃SbSe₃ and Cu₃SbSe₄ samples at room temperature. The actual composition of Cu₃SbSe₃ and Cu₃SbSe₄ samples was determined using Flame atomic absorption spectrometry technique (Analytik Jena, Vario-6) and both the samples exhibited almost the same stoichiometry as the starting composition. Cu₃SbSe₃ crystallize in single-phase with orthorhombic structure with *Pnma* (62) space group with lattice constants[5] of a = 7.98 Å, b = 10.61 Å, c = 6.83 Å, and $\alpha = \beta = \gamma = 90°$. On the other hand, Cu₃SbSe₄ crystallize in a tetragonal structure with $I\bar{4}2m$(121) space group with lattice constants of a = 5.7 Å, b = 5.7 Å, c = 11.2 Å, and $\alpha = \beta = \gamma = 90°$.[12] The high intensity peaks in the XRD patterns clearly indicate the high cystallinity of both the

---

a)Author to whom correspondence should be addressed. Electronic mail: adhar@nplindia.org. Tel.: +91 11 4560 9455/9456. Fax: +91 11 4560 9310

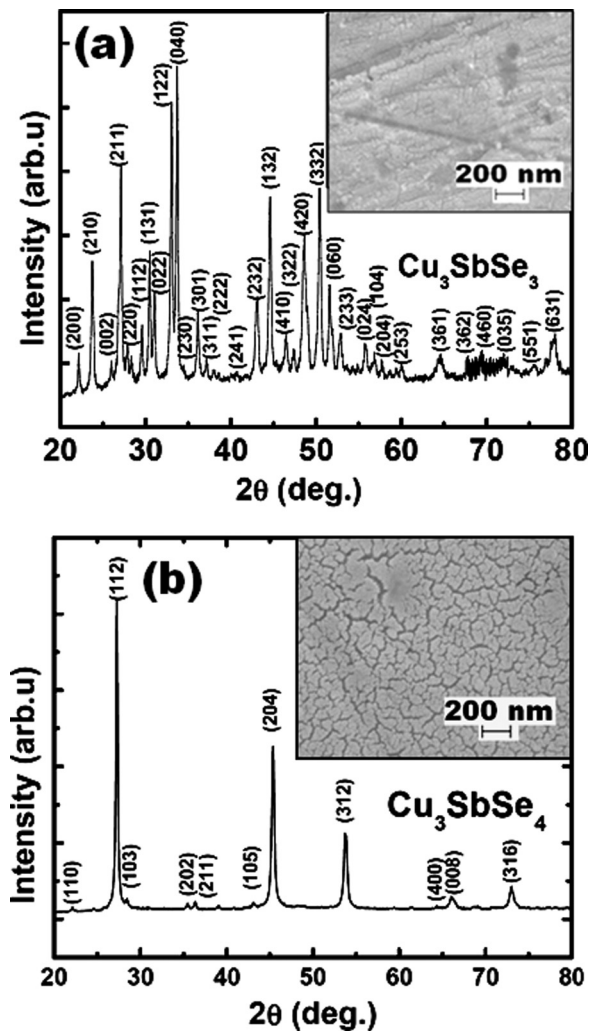FIG. 1. XRD patterns of (a) Cu_3SbSe_3 and (b) Cu_3SbSe_4. Inset of 1(a) and (b) shows the FESEM images of Cu_3SbSe_3 and Cu_3SbSe_4, respectively.

as-synthesized samples. Instrumental broadening has been taken into account while calculating the crystallite sizes of these samples. Further, average crystallite sizes of Cu_3SbSe_3 and Cu_3SbSe_4 samples, as determined using Williamson-Hall method,[13] were found to be ~75 nm and ~102 nm, respectively, which suggests that the as-synthesized samples possess intrinsic nanoscale features.

Field emission scanning electron microscope (FESEM) images of Cu_3SbSe_3 and Cu_3SbSe_4 compounds, shown as insets (a) and (b), respectively, in Fig. 1, confirm their intrinsic nanoscale microstructure. The crystallite size of these compounds, measured by using a linear intercept method, was found to be 80 and 100 nm for Cu_3SbSe_3 and Cu_3SbSe_4, respectively, which are quite close to those obtained using XRD analysis. The grain refinement could be attributed to the presence of Sb in these two compounds, which is well known to be grain refiner.[10,14]

Fig. 2 shows the temperature dependence of electrical and thermal transport properties of Cu_3SbSe_3 and Cu_3SbSe_4 samples. Fig. 2(a), which shows the temperature dependence of Seebeck coefficient for Cu_3SbSe_3 and Cu_3SbSe_4 samples, exhibits a p-type conduction in both the compounds suggesting that the majority carriers are holes. The nearly linear temperature dependence of Seebeck coefficient in Cu_3SbSe_3

is consistent with the picture of a degenerate semiconductor where carrier mean free path is nearly equal to inter-atomic distance. Further, as is evident from Fig. 2(a), the Seebeck coefficient of Cu_3SbSe_4 is higher than Cu_3SbSe_3 sample in the entire temperature range. This higher magnitude of Seebeck coefficient of Cu_3SbSe_4 can be attributed to its crystal structure,[7,9] consisting of a three-dimensional Cu/Se framework [Cu_3Se_4] acting as the hole conduction pathway and the [$SbSe_4$] tetrahedral that is a distorted diamond-like structure, thus, providing a relatively large Seebeck coefficient. The magnitude of the Seebeck coefficient of the Cu_3SbSe_4 sample is comparable to earlier reported values[9,15] (Table I). Whereas, no such reports for Cu_3SbSe_3 is available in literature.[5] Fig. 2(b) shows that the electrical conductivity of Cu_3SbSe_4 is higher than the Cu_3SbSe_3, throughout the temperature range of measurement. Further, in contrast to the Cu_3SbSe_3 sample, the Cu_3SbSe_4 sample exhibits an increase in electrical conductivity with increasing temperature indicating a semiconductor behavior. The electrical conductivity of Cu_3SbSe_4 sample is 3 times higher at 300 K and around an order of magnitude higher at 550 K than that of Cu_3SbSe_3 (Fig. 2(b)).

The variation of thermal conductivity with temperature for both, Cu_3SbSe_3 and Cu_3SbSe_4 samples, has been shown in Fig. 2(c), which clearly exhibits a discontinuity[5] at ~450 K in case of Cu_3SbSe_3 due to a order-disorder transition.[5] The value of thermal conductivity for Cu_3SbSe_3 was found[5] to be $0.26\,W\,m^{-1}\,K^{-1}$ as compared to $0.761\,W\,m^{-1}\,K^{-1}$ for Cu_3SbSe_4 at 550 K. This ultralow value of thermal conductivity in Cu_3SbSe_3 has been attributed to a combination of its complex crystal structure, very low Debye temperature, and extreme anharmonicity of the lattice vibrational spectrum that gives rise to a large value Gruneisen parameter in this compound.[7] On the other hand, Cu_3SbSe_4 sample exhibits the value of κ, which is much lower than reported earlier by Wei *et al.*[15] and Yang *et al.*[6] of 1.35 and $1.1\,W\,m^{-1}\,K^{-1}$, respectively. After combining the results of electrical conductivity, Seebeck coefficient and thermal conductivity, the calculated ZT has been displayed in Fig. 2(d). Despite the intrinsically low value of thermal conductivity in case of Cu_3SbSe_3, a drastic decrease in its electrical conductivity is the main reason for its low value of ZT as compared to Cu_3SbSe_4, which shows a value of 0.3 at 550 K. For better evaluation of our results, we have compared the ZT data of Cu_3SbSe_4 with the recent reports literature,[6,15] as shown in Table I.

Nanoindentation on Cu_3SbSe_3 and Cu_3SbSe_4 compounds was carried out using Berkovich indentor. Hardness and modulus of elasticity (E) measurements were done using Oliver and Pharr method,[16] in which the Sneddon's elastic solution

TABLE I. Current thermoelectric properties of Cu_3SbSe_4 compared with best reported values of similar alloy composition in literature.

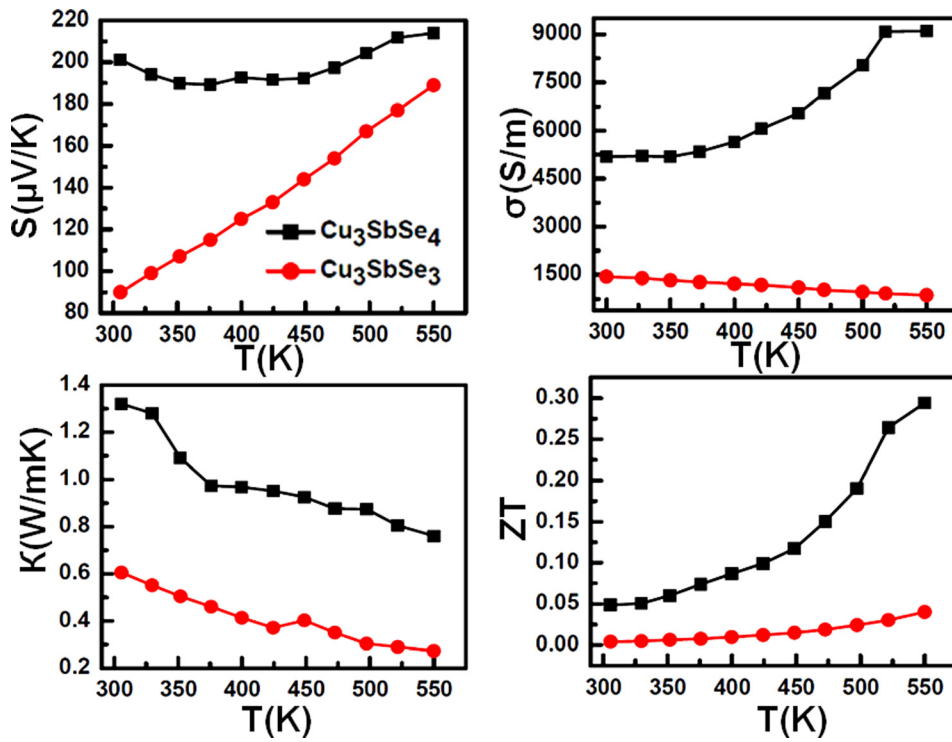| Material	T (K)	Seebeck (μV/K)	κ ($W\,m^{-1}\,K^{-1}$)	σ ($\times 10^3$ S/m)	ZT	Reference
Cu_3SbSe_4	550	214	0.761	9.1	0.30	Current Study
Cu_3SbSe_4	527	347	1.42	4.6	0.20	[15]
Cu_3SbSe_4	575	270	1.1	5	0.19	[4]

FIG. 2. Temperature dependence of thermoelectric properties of Cu_3SbSe_3 and Cu_3SbSe_4 (a) Seebeck coefficient, (b) electrical conductivity, (c) thermal conductivity, and (d) figure-of-merit.

for the indentation of an isotropic sample[17] is used to relate the contact stiffness and the projected contact area between indenter and sample to the indentation modulus, and is given by

$$E = \frac{s}{2\beta}\sqrt{\frac{\pi}{A}}, \qquad (1)$$

where $\beta = 1.034$ for Berkovich indenter and A is the area of indentation, which is given by

$$A = 3\sqrt{3}h_c^2 \tan^2\theta, \qquad (2)$$

where a semi-angle $\theta = 65.3°$ for diamond tip is used. AFM images of Cu_3SbSe_3 and Cu_3SbSe_4 sample after fine polishing and surfaces with indentation marks at different loads given in volts (2 V, 2.5 V, and 3 V) has been shown as an inset of Figs. 3(a) and 3(b). From Figs. 3(a) and 3(b), the unloading curve of load vs distance plot for a trig threshold of 1.5 V, the maximum load P_{max}, and maximum depth of indentation h_{max} is estimated for both Cu_3SbSe_3 and Cu_3SbSe_4 systems. The plastic deformation depth h_f is measured from the point of no load. From the F-D plot, the slope near maximum load $S = dP/dh$ gives the contact stiffness. The contact depth h_c is given by

$$h_c = h - \varepsilon\frac{P}{S}, \qquad (3)$$

where ε is 0.75 for Berkovich[16] indentor. From the F-D plot, considering the elastic deflection of the surface, the critical depth of indentation, h_c is calculated. The hardness of the sample is given by

$$H = \frac{P}{24.5h_c^2}. \qquad (4)$$

From the above analysis of F-D curves, the hardness and modulus of elasticity for Cu_3SbSe_3 and Cu_3SbSe_4 was found

to be 0.85 GPa, 0.63 GPa and 0.39 GPa, 1.06 GPa, respectively. The measured Vickers hardness (VHN) found to be 0.9 GPa and 0.65 for Cu_3SbSe_3 and Cu_3SbSe_4, respectively. This suggests that the hardness values measured by AFM were in fair agreement with the Vickers hardness values. Further, the hardness of Cu_3SbSe_3 samples is much higher than Cu_3SbSe_4 as well as to those of reported for other state-of-the-art TE materials[18,19] as shown in inset of Fig. 4(a). All these reported values are within 5% of uncertainty.
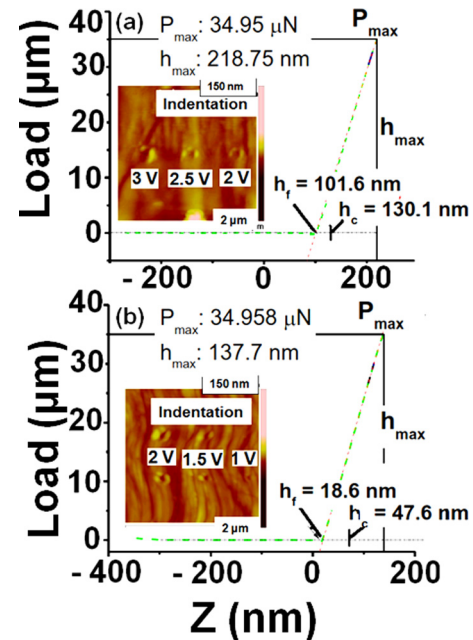

FIG. 3. F-D curve for (a) Cu_3SbSe_3 and (b) Cu_3SbSe_4 showing the unloading part for Trig threshold of 1.5 V. Inset of (a) AFM images of Cu_3SbSe_3 and inset of (b) Cu_3SbSe_4 samples with indentation marks at different loads given in volts (2 V, 2.5 V, and 3 V).

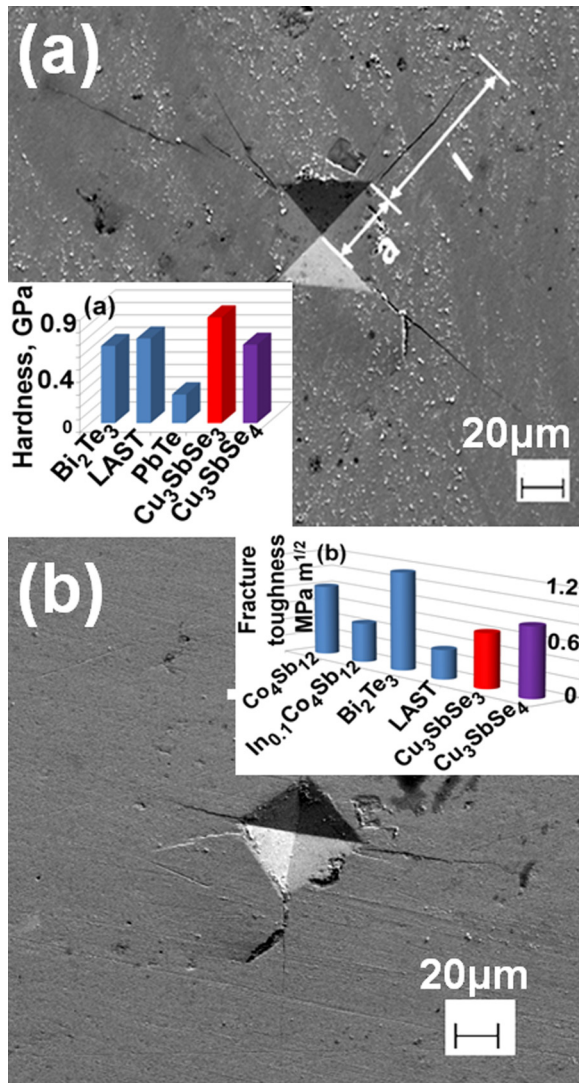FIG. 4. FESEM images of Vickers-indentation cracks developed in (a) Cu_3SbSe_3 (b) Cu_3SbSe_4. Indentation crack length '*l*' and the half-diagonal of indentation '*a*' is marked. Inset of (a) and (b) is the hardness and fracture toughness of Cu_3SbSe_3 and Cu_3SbSe_4, respectively, compared with the reported values of state-of-the-art and competing thermoelectric materials.

Fracture toughness was estimated by a method proposed by Niihara *et al.*,[20] which is quite accurate and successful for a range of brittle materials. According to this method, the fracture toughness (K_{IC}), as measured by Vicker's indentation-crack technique with Palmqvist crack model[21] is given as

$$K_{IC} = 0.0089 \left(\frac{E}{H}\right)^{2/5} \times \frac{P}{al^{1/2}}; \quad 2.5 \geq \frac{l}{a} \geq 0.25,$$

where *P* is the load, *l* is the crack length, *a* is half-diagonal of Vicker's indentation, *E* is the Young's modulus, and *H* is the hardness. In the present work, dimensions "*a*" and "*l*" were measured using FESEM for better accuracy of the results (Figs. 4(a) and 4(b)). The calculated fracture toughness of Cu_3SbSe_3 and Cu_3SbSe_4 found to be 0.63 ± 0.05 and 0.80 ± 0.03 MPa m$^{1/2}$, respectively, which are comparable with the other state-of-the-art TE materials[18,22] (as shown in inset of Fig. 4(b)). Moreover, it is well known that the fine grain size in nanostructured alloys helps to minimize the dislocation pile-up stresses resulting in improvement in fracture

toughness.[23] In the present study, it has been observed that the intrinsically nanostructure of Cu_3SbSe_3 and Cu_3SbSe_4 sample is expected to assist in localized fracture processes, which generally occurs during crack extension in many nanostructured materials and which in turn improves the fracture toughness.[24] Furthermore, fracture toughness of the materials could also be improved by the addition of nano-sized secondary reinforcements without losing its transport properties, where these reinforcements act as crack bridging and crack deflection.[25]

It is well known that in order to enhance the efficiency of TE devices the segmentation of the thermoelectric elements is desirable,[26,27] which is judged by the thermoelectric compatibility factor of the material, given as[28]

$$S = \frac{\sqrt{1 + ZT} - 1}{\alpha T},$$

where α is Seebeck coefficient in Volts and T is temperature in Kelvin.

The thermoelectric compatibility of thermoelectric materials[24] is currently of technological interest in TE device fabrication for enhancement of their efficiency.[28] However, in order to derive a maximum TE efficiency benefit of employing segmentation in TE devices, the difference in compatibility factor (S) for the two TE materials should be less than a factor of 2.[26,28] The temperature dependence of TE compatibility factor for Cu_3SbSe_3 and Cu_3SbSe_4 sample are shown in Fig. 5. It is clear from this figure that the compatibility factor of Cu_3SbSe_3 is quite low ~0.2 V^{-1} as compared to 1.2 V^{-1} for Cu_3SbSe_4 at 550 K. In comparison to other state-of-the art p-type TE materials,[29] the compatibility factor of Cu_3SbSe_4 is reasonably good thus making it a suitable candidate for segmentation with other TE materials to derive enhanced efficiency benefit. However, the compatibility factor of these materials can further be enhanced by increasing their ZT employing suitable doping and adopting nanostructuring.

In summary, Cu_3SbSe_3 and Cu_3SbSe_4 thermoelectric compounds were synthesized by conventional fusion method followed by spark plasma sintering. Cu_3SbSe_4 exhibits a much higher ZT compared to Cu_3SbSe_3, which is due to its large electrical conductivity. Mechanical properties, in terms

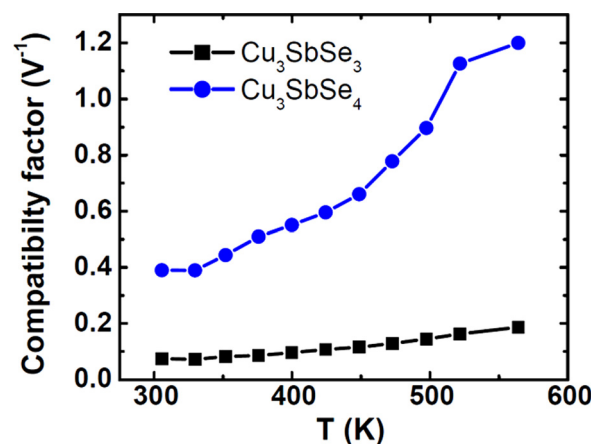FIG. 5. Thermoelectric compatibility factor for Cu_3SbSe_3 and Cu_3SbSe_4, as a function of temperature.

of hardness and fracture toughness, were measured using both Berkovich and Vickers indentors. Hardness and fracture toughness values for Cu_3SbSe_3 and Cu_3SbSe_4 were found to be 0.9 GPa, 0.65 GPa and 0.63 MPa m$^{1/2}$, 0.80 MPa m$^{1/2}$, respectively, which are superior compared to the existing state-of-the-art TE materials. The TE compatibility factor of Cu_3SbSe_4 was found to be 1.2 V^{-1}, which is much higher than 0.2 V^{-1} for Cu_3SbSe_3, which is mainly due to its higher ZT, owing to its higher electrical conductivity in comparison to Cu_3SbSe_3. Thermoelectric and mechanical properties of these materials can be improved further by suitable doping and nanostructuring methodology.

[1]T. M. Tritt and M. A. Subramanian, MRS Bull. **31**(03), 188 (2006); T. M. Tritt *Thermal Conductivity: Theory, Properties, and Applications* (Academic Press, San Diego, CA, 2000); D. M. Rowe, *Thermoelectrics Handbook: Macro to Nano* (CRC Press, 2005).

[2]A. F. Ioffe, *Semiconductor Thermoelements, and Thermoelectric Cooling* (Infosearch ltd., 1957); S. Bathula, M. Jayasimhadri, N. Singh, A. K. Srivastava, J. Pulikkotil, A. Dhar, and R. C. Budhani, Appl. Phys. Lett. **101**(21), 213902 (2012); K. Tyagi, B. Gahtori, S. Bathula, S. Auluck, and A. Dhar, *ibid.* **105**(17), 173905 (2014).

[3]G. D. Mahan, Solid State Phys. **51**, 81 (1997).

[4]E. J. Skoug, J. D. Cain, D. T. Morelli, M. Kirkham, P. Majsztrik, and E. Lara-Curzio, J. Appl. Phys. **110**(2), 023501 (2011); E. J. Skoug, J. D. Cain, and D. T. Morelli, Appl. Phys. Lett. **96**(18), 181905 (2010); E. J. Skoug, J. D. Cain, P. Majsztrik, M. Kirkham, E. Lara-Curzio, and D. T. Morelli, Sci. Adv. Mater. **3**(4), 602 (2011); E. J. Skoug and D. T. Morelli, Phys. Rev. Lett. **107**(23), 235901 (2011).

[5]K. Tyagi, B. Gahtori, S. Bathula, A. K. Srivastava, A. K. Shukla, S. Auluck, and A. Dhar, J. Mater. Chem. A **2**(38), 15829 (2014).

[6]C. Yang, F. Huang, L. Wu, and Ke. Xu, J. Phys. D: Appl. Phys. **44**(29), 295404 (2011).

[7]Y. Zhang, E. Skoug, J. Cain, V. Ozoliņš, D. Morelli, and C. Wolverton, Phys. Rev. B **85**(5), 054306 (2012).

[8]C. Sevik and T. Çağın, J. Appl. Phys. **109**(12), 123712 (2011); H. Nakanishi, S. Endo, and T. Irie, Jpn. J. Appl. Phys., Part 1 **8**(4), 443 (1969); O. Madelung, *Semiconductors: Data Handbook* (Springer, 2004).

[9]E. J. Skoug, J. D. Cain, and D. T Morelli, Appl. Phys. Lett. **98**(26), 261911 (2011).

[10]Q. Wang, W. Chen, W. Ding, Y. Zhu, and M. Mabuchi, Metall. Mater. Trans. A **32**(13), 787 (2001).

[11]Y. Liu, J. Yang, E. Gu, T. Cao, Z. Su, L. Jiang, C. Yan, X. Hao, F. Liu, and Y. Liu, J. Mater. Chem. A **2**(18), 6363 (2014).

[12]J. Garin and E. Parthe, Acta Crystallogr., Sect. B: Struct. Crystallogr. Cryst. Chem. **28**(12), 3672 (1972).

[13]S. Bathula, R. C. Anandani, A. Dhar, and A. K. Srivastava, Mater. Sci. Eng. A **545**, 97 (2012); K. Venkateswarlu, A. C. Bose, and N. Rameshbabu, Physica B: Condens. Matter **405**(20), 4256 (2010).

[14]Y. Q. Ma, R. S. Chen, and En.-H. Han, Mater. Lett. **61**(11), 2527 (2007).

[15]T.-R. Wei, H. Wang, Z. M. Gibbs, C.-F. Wu, G. J. Snyder, and J.-F. Li, J. Mater. Chem. A **2**(33), 13527 (2014).

[16]W. C. Oliver and G. M. Pharr, J. Mater. Res. **7**(06), 1564 (1992).

[17]I. N. Sneddon, Int. J. Eng. Sci. **3**(1), 47 (1965).

[18]Li.-D. Zhao, Bo.-P. Zhang, J.-F. Li, M. Zhou, W.-S. Liu, and J. Liu, J. Alloys Compd. **455**(1), 259 (2008); P. Miao, G. R. Odette, T. Yamamoto, M. Alinger, D. Hoelzer, and D. Gragg, J. Nucl. Mater. **367**, 208 (2007).

[19]F. Ren, E. D. Case, E. J. Timm, and H. J. Schock, J. Alloys Compd. **455**(1), 340 (2008).

[20]K. Niihara, R. Morena, and D. P. H. Hasselman, J. Mater. Sci. Lett. **1**(1), 13 (1982).

[21]S. Palmqvist, Jernkontorets Ann. **141**, 300 (1957); Z. Li, A. Ghosh, A. S. Kobayashi, and R. C. Bradt, J. Am. Ceram. Soc. **72**(6), 904 (1989).

[22]J. R. Salvador, J. Yang, X. Shi, H. Wang, A. A. Wereszczak, H. Kong, and C. Uher, Philos. Mag. **89**(19), 1517 (2009).

[23]A. C. Kallel, G. Roux, and C. L. Martin, Mater. Sci. Eng. A **564**, 65 (2013); J.-F. Li, W.-S. Liu, Li.-D. Zhao, and M. Zhou, NPG Asia Mater. **2**(4), 152 (2010).

[24]S. Bathula, B. Gahtori, M. Jayasimhadri, S. K. Tripathy, K. Tyagi, A. K. Srivastava, and A. Dhar, Appl. Phys. Lett. **105**(6), 061902 (2014).

[25]J. Eilertsen, M. A. Subramanian, and J. J. Kruzic, J. Alloys Compd. **552**, 492 (2013); R. A. Varin, L. Zbroniec, T. Czujko, and Y.-K. Song, Mater. Sci. Eng. A **300**(1), 1 (2001).

[26]G. J. Snyder and T. S. Ursell, Phys. Rev. Lett. **91**(14), 148301 (2003).

[27]G. J. Snyder, Appl. Phys. Lett. **84**(13), 2436 (2004).

[28]E. Maciá, Phys. Rev. B **70**(10), 100201 (2004).

[29]P. H. Ngan, D. V. Christensen, G. J. Snyder, Le. T. Hung, S. Linderoth, N. Van Nong, and N. Pryds, Phys. Status Solidi A **211**(1), 9 (2014).